

Electron-impact ionization of iron ions: Fe¹¹⁺, Fe¹³⁺, and Fe¹⁵⁺

D. C. Gregory, L. J. Wang, and F. W. Meyer

Physics Division, Oak Ridge National Laboratory, Oak Ridge, Tennessee 37831-6372

K. Rinn

Joint Institute for Laboratory Astrophysics, Boulder, Colorado 80309-0440

and Oak Ridge National Laboratory, Oak Ridge, Tennessee 37831-6372

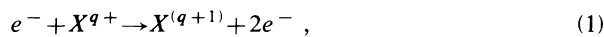
(Received 21 November 1986)

Absolute cross-section measurements are reported for electron-impact ionization of iron ions with initial charges 11+, 13+, and 15+. The data extend from below the ionization thresholds to 1500 eV for Fe¹¹⁺ and to 1400 eV for Fe¹³⁺, while the Fe¹⁵⁺ data cover the energy range from 630 to 1000 eV. Good agreement is found in each case between the measurements and detailed calculations which include the contributions due to the mechanism of inner-shell excitation-autoionization, but predicted significant enhancements of the Fe¹⁵⁺ cross section due to resonant-excitation double autoionization are not observed. Ionization rate coefficients and fitting parameters are presented based on the data.

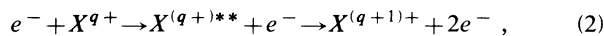
I. INTRODUCTION

Highly charged ions play an important role in astrophysical and laboratory plasmas. Modeling studies of power balance, equilibrium charge states and temperatures, and the interpretation of diagnostic information from injected impurities all depend in part on an accurate data base of rate coefficients for electron-impact excitation, ionization, and recombination.¹⁻³ In order to develop this data base, accurate cross-section measurements and calculations are necessary to provide specific data⁴ as well as a basis for the formulation of general scaling laws.

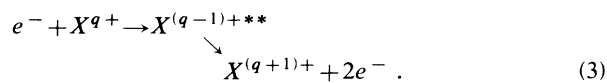
There are a number of processes that may contribute to the production of a particular final state of the target ion, and the relative importance of each of these processes may change with the target-ion charge or electronic structure. Ionization of a target ion may occur through direct removal of an electron,



through excitation of an inner-subshell target electron followed by autoionization, as illustrated by



or through excitation of a target electron accompanied by capture of the incoming electron followed by double autoionization,



Other exotic processes have been predicted to contribute significantly to the total net ionization,⁵ but this work will concentrate on the above possibilities. In the notation used here, process (1) refers to direct ionization, process (2) to excitation-autoionization (EA), and the series of

events in process (3) will be termed resonant-excitation double autoionization⁶ (REDA). The relative importance of each process changes with each ion studied, and in principle even pathway (3) could dominate total ionization over a limited energy range for a specific ion. In general, indirect processes such as those shown in Eqs. (2) and (3) have been found to become relatively more important as the charge and mass of the target ion increase.^{7,8} This is because the peak direct-ionization cross section decreases faster than most inner-shell excitation cross sections as the ionic charge increases. Sudden changes in the indirect contribution may be observed along isoelectronic (same number of electrons) and isonuclear (same element) sequences as previously autoionizing excited configurations become bound, and slower changes occur as branching ratios alter the preferred exit channels. The importance of such trends along sequences is well recognized and a high priority has been given to measurements of ionization cross sections for specific highly charged ions.⁹ The iron isonuclear sequence is one of the most important for the fusion effort, since any plasma contained in a stainless-steel vessel is likely to contain iron impurities. Iron is also an abundant element in astrophysical plasmas.

Ion beams of metallic elements are generally more difficult to produce than beams from elements which naturally occur in a gaseous state, either as free atoms or in simple molecules. For this reason, much of the previous work¹⁰ on electron-impact processes studied by crossed-beam experiments has dealt with light elements ($z < 9$) and inert gases. The alkali-metal elements have also been popular because relatively simple ion sources may be made for these elements. Metal ions have been much less extensively studied, and no crossed-beam measurements had been reported involving metallic ions of initial charge greater than 3+ until recently. For iron, ionization cross-section measurements have been reported¹¹⁻¹³ for charge states 1+, 2+, 5+, 6+, and 9+. Among the theoretical studies of ionization of iron ions, we note the

distorted-wave calculations of Younger,¹⁴ Griffin *et al.*,¹⁵ and the recent more extensive work of Pindzola *et al.*¹⁶

Na-like ions, with one electron outside a closed shell, have proved to be important in plasma studies and amenable to calculation. In ionization and excitation of Na-like ions, Fe¹⁵⁺ is particularly important due to its expected presence in laboratory plasmas. Mann,¹⁷ among others, has studied excitation of Fe¹⁵⁺, and Cowan and Mann¹⁸ published detailed calculations predicting that excitation-autoionization effects would dominate total ionization for Fe¹⁵⁺. This was followed by an even more surprising prediction by LaGattuta and Hahn¹⁹ that resonant-excitation double autoionization would dominate (over a relatively small energy range) the total ionization cross section. Measurements on electron-impact ionization of Fe¹⁵⁺ have been considered an important and critical test of theory since that time.

We present here an extension of previous measurements¹³ for ionization of multiply charged iron ions to higher charge states with absolute data for single ionization of Fe¹¹⁺, Fe¹³⁺, and Fe¹⁵⁺ by electron impact. The experimental arrangement and uncertainties are discussed in Sec. II, results for these ions are presented and discussed in Sec. III, rate coefficients and analytical fits are given in Sec. IV, and the summary and conclusions are in Sec. V.

II. EXPERIMENTAL ARRANGEMENT AND UNCERTAINTIES

General tutorials concerning the techniques and sources of uncertainty in electron-ion crossed-beam experiments are available^{20,21} and a detailed description of the apparatus used in these experiments has recently been published.¹³ The present discussion will provide a brief overview of the experimental arrangement and uncertainties, with emphasis on those details unique to these measurements.

Absolute cross-section measurements depend on the event rate, particle currents and velocities, and the overlap of the intersecting beams (an alternative technique²² sweeps one beam across the other). For electron and ion beams crossing at 90°, the absolute cross section $\sigma(E)$ at an interaction energy E is determined from these quantities through the relation

$$\sigma(E) = \frac{Rqe^2}{I_i I_e} \frac{v_i v_e}{(v_i^2 + v_e^2)^{1/2}} \frac{F}{D}, \quad (4)$$

where R is the signal event rate, q is the charge on the in-

cident ion, e is the charge on an electron, v_i and v_e are the ion and electron velocities, I_i and I_e are ion and electron currents, D is the probability of detecting and counting a signal event, and F is the form factor which takes into account the spatial overlap of the ion and electron beams. The apparatus is designed to allow precise measurements of each of these quantities over an extended energy range; typical values for each ion are listed in Table I.

The apparatus is shown in Fig. 1. Ions were extracted at 10-kV potential from the Oak Ridge National Laboratory Electron Cyclotron Resonance (ORNL-ECR) source,²³ analyzed for the desired ratio of charge to mass, and transported to the ultrahigh-vacuum chamber. One-dimensional einzel lenses provided steering and focusing of the beam, which then passed through a 90° electrostatic analyzer (labeled purifier in Fig. 1) to remove any ions which changed charge during the flight from the source. After passing through the interaction volume located at the center of the electron gun, the beam was analyzed in a double-focusing magnetic analyzer to separate the further-ionized ions from the parent ion beam. These “signal” ions were electrostatically deflected out of the analyzer plane and counted in the ionized-ion detector (a channel-electron multiplier). This final 90° deflection is represented in Fig. 1 as being in the analyzer plane for simplicity. The unchanged ion beam was collected in one of two movable Faraday cups, depending on the ratio of incident to product ion charge. Peak ion-beam currents in the collision chamber for these ions ranged from 0.5 to 3 particle nA.

The electron gun is almost identical to that described by Taylor *et al.*^{24,25} and produces a beam immersed in a 250-G axial magnetic field. This confining field enhances the uniformity of the beam density and its physical size at the collision volume over a wide range of electron beam energies. Electrons are collected in an array of edge-forward tantalum “razor blades” which minimize the escape of backscattered electrons. The collector is normally biased at +300 V or one-half the beam energy (whichever is greater) to prevent the escape of secondary electrons. The electron beam is chopped by applying sufficient negative voltage to one of the electrodes upstream of the collision volume so that the beam is prevented from passing through this electrode. Energy spread in the beam is estimated from other experiments to be between 1 and 2 eV at the energies used in these experiments.²⁶

Determination of the cross section through Eq. (4) involves straightforward measurements of ion-beam current, electron-beam current, and the accelerating voltages for

TABLE I. Typical experimental parameters. Currents and event rates are shown for typical measurements at approximately twice the listed ground-state ionization thresholds.

Ion	Ionization potential (eV)	Ion current (particle nA)	Electron current (mA)	Form factor (cm)	Background event rate (Hz)	Signal event rate (Hz)
Fe ¹¹⁺	331	1.8	5.4	0.40	139.0	11.0
Fe ¹³⁺	392	0.38	6.3	0.42	73.0	1.6
Fe ¹⁵⁺	489	0.38	9.8	0.47	34.0	1.4

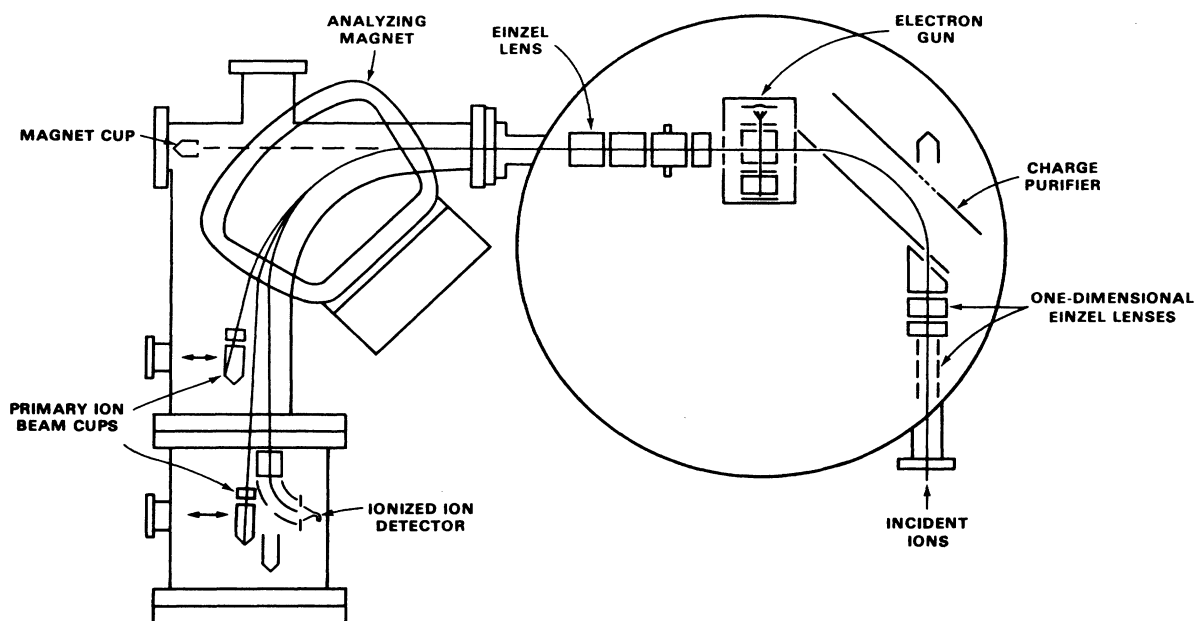


FIG. 1. Schematic of the crossed-beam collision chamber and post-collision magnetic charge analyzer.

these beams. In addition, the signal event rate is determined by subtracting the detector count rate measured with the electron beam off from the rate measured when the electron beam is on. Small corrections are made to the net event rate for possible incomplete transmission of ions to the detector, detection efficiency of the detector, and pulse transmission of the electronics, all of which are incorporated into the factor D (typically 0.95) in Eq. (4). The form factor F is calculated based on ion- and electron-beam spatial profiles, which are obtained by measuring the currents transmitted through a narrow slit in a probe as it is scanned through each beam in the interaction volume. A form factor is derived from these spatial profiles through the relation

$$F = \frac{\int I_i(z) dz \int I_e(z) dz}{\int I_i(z) I_e(z) dz}, \quad (5)$$

where $I_i(z)$ and $I_e(z)$ are the measured profiles, and z is perpendicular to the plane of intersection of the beams.

Uncertainties reported in the data table and shown in the figures are relative only at the 1-standard-deviation (s.d.) level, and are strongly dominated by statistical uncertainties in the signal count rate. In addition, some uncertainties are common to all of the measurements for a given ion, and the overall uncertainty in the magnitude of the cross sections must include these "systematic" uncertainties.

Table II lists the sources of systematic uncertainty iden-

TABLE II. Absolute uncertainties. All uncertainties are "good" confidence level (equivalent to 90% confidence level on statistical uncertainties).

Source	Uncertainty (%)		
	Fe ¹¹⁺	Fe ¹³⁺	Fe ¹⁵⁺
Counting statistics (typical value near the peak cross section at 90% confidence level)	9	20	20
Form factor (absolute uncertainty)	4	4	4
Transmission of ions to detector	8	8	5
Signal ion detection and pulse transmission	4	4	3
Ion current measurement	2	2	2
Electron current measurement	2	2	2
Ion and electron velocities	1	1	1
Quadrature sum	14%	23%	21%

tified for these experiments, along with the assigned uncertainties at "good" confidence level,²⁷ equivalent to 2 s.d. (or 90% confidence level) on counting statistics. The uncertainties due to counting statistics are taken for single typical points near the peak of each cross section. The uncertainty in form factor takes into account potential systematic problems in the measurement of beam profiles and numerical determination of the overlap integral. The transmission of all signal ions to the detector is normally monitored by scanning critical beam tuning parameters while monitoring the effective signal level; however, the combination of weak beams and high backgrounds for Fe¹¹⁺ and Fe¹³⁺ precluded extensive scans. Tuning parameters in this apparatus have been found to be only weakly dependent on ion-charge state; we therefore feel justified in using settings determined from diagnostic scans¹³ for Fe⁹⁺ for measurements on Fe¹¹⁺ and Fe¹³⁺. The background event rate (normally dominated by ionization of beam ions on background gas) for Fe¹⁵⁺ was considerably less than that observed for the lower charge states, and complete scans of critical tuning parameters were performed as previously described. The detection efficiency of the channel-electron multiplier for energetic ions is assumed to be near unity based on independent published measurements.²⁸⁻³⁰ Pulse transmission through the detection electronics was measured for each

of these ions, and appropriate corrections made to the signal count rates. Ion and electron currents and velocities were measured. The quadrature sum of these uncertainties for each ion is considered a conservative absolute uncertainty at good confidence level, since taking the relative uncertainty of a single point underestimates our confidence in the overall shape of the cross-section curve.

III. RESULTS AND DISCUSSION

A. Fe¹¹⁺

Experimental cross sections for ionization of Fe¹¹⁺ are listed in Table III and plotted in Figs. 2 and 3. The uncertainties listed and plotted are 1 s.d. relative only, and are dominated by counting statistics. Total absolute uncertainty for a typical measurement near the peak cross section is 14% at 90% confidence level (see Table II). All measurements are shown in Fig. 2, along with distorted-wave calculations for direct ionization from ground-state¹⁴ ($3s^33p^3$, lower curve) and metastable³¹ ($3s^23p^23d$, upper curve) incident ions. In the energy range below 700 eV, direct ionization from the ground ($3s^23p^3$) configuration consistently underestimates the measured cross section, with experiment 30% above theory at 700 eV. In the same energy range, direct ionization from the $3s^23p^23d$

TABLE III. Experimental electron-impact ionization cross sections for Fe¹¹⁺, Fe¹³⁺, and Fe¹⁵⁺. Uncertainties listed here are 1 s.d. relative only.

Fe ¹¹⁺		Fe ¹³⁺		Fe ¹⁵⁺	
Energy (eV)	Cross section (10 ⁻¹⁸ cm ²)	Energy (eV)	Cross section (10 ⁻¹⁸ cm ²)	Energy (eV)	Cross section (10 ⁻¹⁸ cm ²)
293	0.02±0.05	342	-0.04±0.09	634.2	0.071±0.048
317	-0.02±0.07	392	-0.006±0.077	686.1	0.076±0.042
342	0.19±0.06	416	0.02±0.14	727.3	0.058±0.043
391	0.36±0.05	442	0.28±0.08	741.5	0.155±0.046
440	0.52±0.06	490	0.21±0.10	751.1	0.105±0.026
490	0.60±0.06	540	0.27±0.09	757.0	0.151±0.026
540	0.73±0.04	590	0.13±0.08	760.4	0.172±0.032
590	0.79±0.04	639	0.20±0.11	769.1	0.190±0.056
639	0.80±0.04	688	0.38±0.10	778.1	0.175±0.043
664	0.83±0.05	739	0.44±0.08	785.7	0.242±0.046
688	0.84±0.06	763	0.50±0.09	796.6	0.198±0.051
713	0.90±0.05	788	0.68±0.08	800.9	0.317±0.042
738	0.95±0.04	838	0.71±0.06	804.8	0.305±0.042
763	1.06±0.05	885	0.78±0.07	805.7	0.250±0.027
788	1.17±0.03	935	0.85±0.10	806.2	0.150±0.050
812	1.09±0.04	986	0.68±0.07	806.7	0.210±0.025
838	1.16±0.04	1086	0.54±0.10	807.3	0.355±0.042
862	1.09±0.05	1183	0.64±0.09	816.0	0.253±0.028
887	1.11±0.04	1282	0.63±0.10	820.8	0.298±0.065
935	1.08±0.05	1381	0.58±0.09	835.2	0.257±0.027
988	1.12±0.04			850.2	0.353±0.033
1039	1.15±0.03			855.6	0.278±0.047
1090	1.04±0.04			870.4	0.287±0.029
1138	1.07±0.05			872.0	0.349±0.045
1189	1.05±0.04			904.5	0.271±0.027
1288	1.04±0.04			924.6	0.302±0.034
1385	0.93±0.04			956.9	0.339±0.034
1481	0.80±0.03			988.0	0.321±0.047

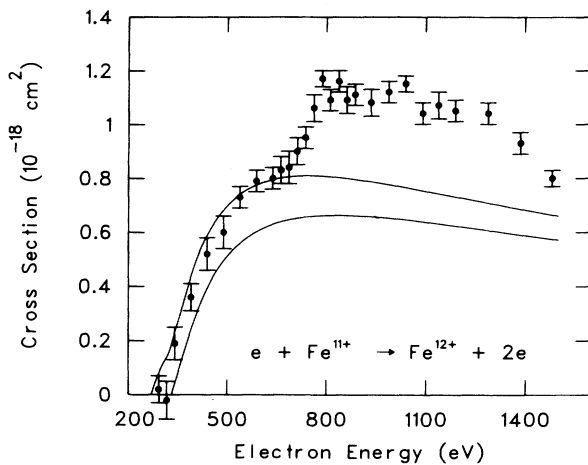


FIG. 2. Cross section vs interaction energy for electron-impact ionization of Fe^{11+} . Plotted uncertainties are 1 s.d. relative only. The solid curves are distorted-wave calculations for direct ionization of ground-state ($3s^23p^3$) ions (lower curve, from Ref. 14) and of metastable ions in a $3s^23p^23d$ configuration (upper curve, from Ref. 31).

metastable configuration appears to agree with experiment, implying that the incident ion beam is dominated by metastables. However, contributions due to excitation of inner-subshell electrons followed by autoionization are predicted³¹ to enhance ionization from the metastable configuration beginning at the ionization threshold at 270 eV, so that total ionization from a 100% metastable ion

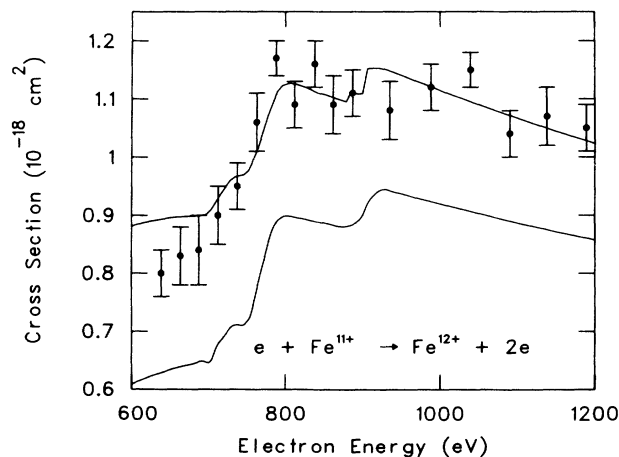


FIG. 3. Comparison of Fe^{11+} data and distorted-wave calculations for total ionization, including direct ionization and excitation-autoionization effects. The calculations (from Ref. 16) include five transitions involving excitation of inner-shell $2p$ and $2s$ electrons. The lower curve is for initially ground-state ($3s^23p^3$) ions, and the upper curve is for metastable ($3s^23p^23d$) ions. Note that additional transitions at lower energies contribute to autoionization of metastable ions.

beam would overestimate the experiment by 60% at 400 eV and by 10% at 700 eV. It seems most reasonable, in light of these comparisons, to conclude that the incident ion beam contains a mixture of ground-state and metastable ions.

The main contributions to excitation-autoionization occur at energies above 700 eV, and the data are compared in Fig. 3 to detailed total ionization calculations which include excitation to any of five autoionizing levels.^{16,31} Results are shown for both metastable- and ground-configuration incident ions. Good agreement is found between experiment and total ionization from metastable ions in this energy range, while the calculations for ground-state ions are uniformly 30% low. The question of metastable fraction restricts the detailed conclusions that can be drawn from this comparison, but good agreement is found between experiment and theory for the magnitude of the excitation-autoionization contribution to the total cross section. Clearly, indirect ionization is important for Fe^{11+} , contributing as much as 30% of the total near the peak cross section.

B. Fe^{13+}

Measurements for ionization of Fe^{13+} are listed in Table III and plotted in Fig. 4. Uncertainties listed and plotted are relative only at the 1-s.d. level, and are larger than those for Fe^{11+} . This is due to a combination of a smaller cross section (the peak direct-ionization cross section for Fe^{13+} is less than half that of Fe^{11+}) and a proportionally larger background count rate (compared to the signal rate), requiring a longer integration time for an equivalent statistical uncertainty. The absolute uncertainty for the cross-section curve (23%) also reflects the larger relative uncertainty (see Table II).

The data are compared in Fig. 4 to calculations of direct ionization (lower solid curve, Ref. 14) of $3s^23p$

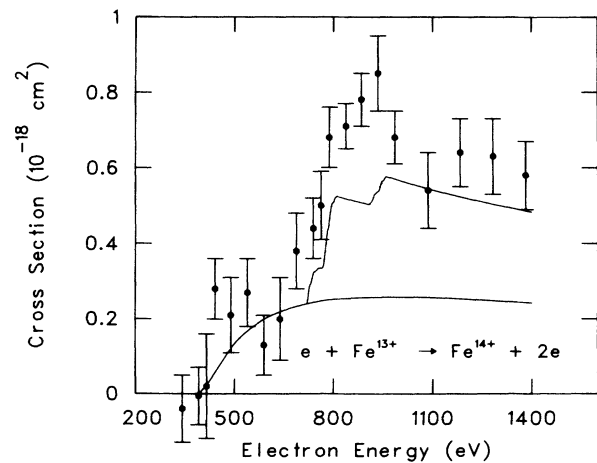


FIG. 4. Electron-impact ionization of Fe^{13+} . The data are compared to distorted-wave calculations for direct ionization of ground-state ($3s^23p$) ions (lower curve, from Ref. 14) and including the effects of excitation-autoionization (upper curve, from Ref. 16).

ground-state ions, and to calculations which include the contributions of excitation to any of five autoionizing configurations (upper solid curve, Ref. 31). Within the stated relative and absolute experimental uncertainties, only general comparisons can be made between theory and experiment. The onset of indirect ionization is observed near 690 eV, in reasonable agreement with theory.³¹ The distorted-wave calculation of direct ionization agrees with experiment at energies where such a comparison can be made (below the threshold for indirect processes). The contribution of excitation-autoionization to the total cross section appears to be underestimated by theory above 800 eV.

The relative importance of indirect ionization is considerably greater for Fe^{13+} than for Fe^{11+} . As has been noted, the peak direct cross section is more than a factor of 2 smaller for Fe^{13+} , but the peak indirect contribution is actually larger than for Fe^{11+} (based on the theory shown in Fig. 4, which may be taken as a lower limit). Thus, while indirect ionization made a 30% contribution to the peak total cross section for Fe^{11+} , it constitutes over half of the total for Fe^{13+} .

C. Fe^{15+}

Measurements of the electron-impact ionization cross section for Fe^{15+} are listed in Table III and plotted in Fig. 5. For this ion, measurements were not made below the ionization threshold due to the prohibitive time which would be required to accumulate the statistics necessary to

accurately determine an experimental threshold. Other evidence suggests the absence of highly excited metastable ions (see the discussion below), and measurements were extended to sufficiently low energies to provide a baseline against which to judge the relative contributions of direct and indirect ionization. Statistical uncertainties are plotted and listed at the 1-s.d. level in Fig. 5 and in Table III, and the absolute uncertainty (in Table II) is dominated by counting statistics. Diagnostic scans of critical tuning parameters were carried out for this ion, despite the fact that the peak measured cross section was a factor of 2 smaller than that for Fe^{13+} , and almost a factor of 4 smaller than for Fe^{11+} . The reduced signal rate was more than compensated for by a small background due to ionization of incident ions by phenomena other than collisions with beam electrons. Even with the small background, over two weeks of measurements were required to complete a set of diagnostic scans (as described in Ref. 13) for Fe^{15+} .

The obvious source of background counts in the signal ion detector is ionization resulting from collisions with residual gas in the collision chamber. A second source of background recently encountered for other Na-like ions stems from production in the ion source of autoionizing metastable ions of the configurations $2p^3 3s nl$, some of which can then spontaneously decay in the vicinity of the collision region and be detected in the signal channel.^{32,33} If the lifetimes of these excited states are long enough that a significant fraction decay after charge-state analysis of the ion beam, and short enough that a significant number

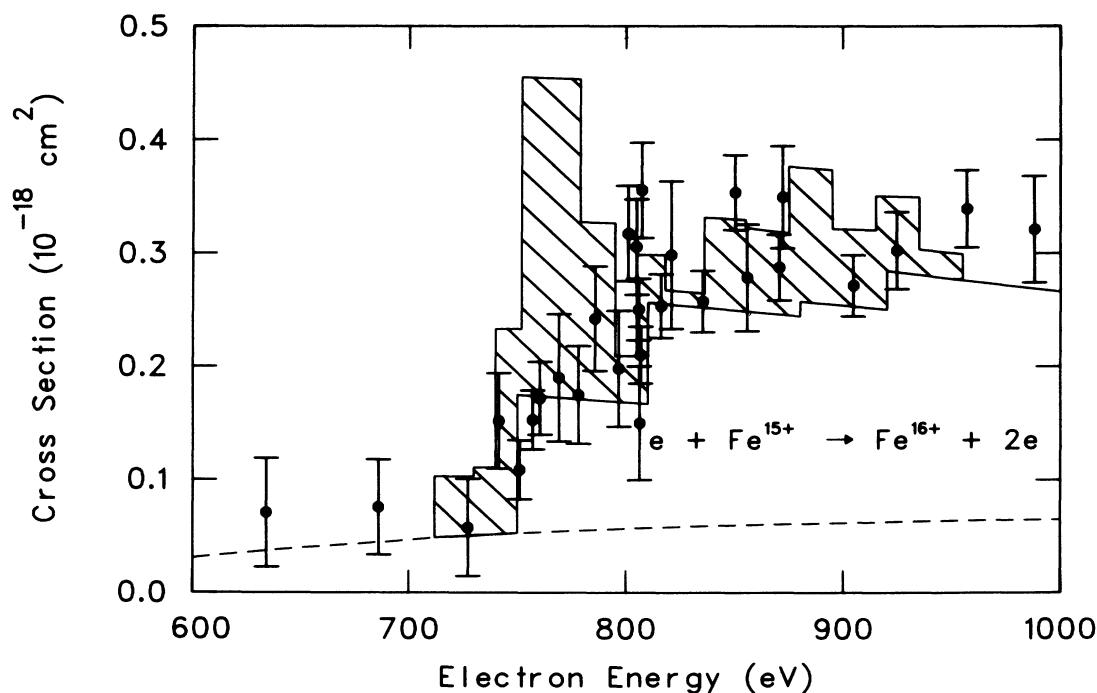


FIG. 5. Electron-impact ionization of Fe^{15+} . Present data compared to Lotz predictions for direct ionization (dashed curve, Ref. 34), direct ionization added to distorted-wave calculations including excitation-autoionization (lower solid curve, Ref. 35), and calculations including resonant-excitation double autoionization (upper solid curve, Ref. 19). The hatched region indicates the predicted cross-section enhancement due to resonant-excitation double autoionization.

decay per centimeter along the flight path near the experiment collision volume, then the background count rate may be large enough to prevent the accumulation of meaningful statistics in a reasonable time. This was the case^{32,33} in our measurements on Na-like ions S^{5+} , Cl^{6+} , and Ar^{7+} . The effect of autoionizing metastable ions in the incident beam was expected to decrease with increasing charge, and apparently for Fe^{15+} either the metastable levels are not populated or have such short lifetimes that a significant number do not survive the flight down the beam line.

The measurements are compared in Fig. 5 to calculations of direct ionization of the outer $3s$ electron (dashed curve, Ref. 34) and to total ionization calculations including excitation of inner-shell $2p$ and $2s$ electrons to autoionizing levels (lower solid curve, Ref. 35). The upper solid curve in Fig. 5 includes predictions of resonant-excitation double autoionization by LaGattuta and Hahn.¹⁹ It is clear that the predicted large enhancement of the cross section due to the REDA process is not observed, at least in the 750–780-eV range where a factor of 2.5 enhancement over the direct ionization plus excitation-autoionization was predicted. The calculations assume a 20-eV electron-energy bin width, while the present experimental energy spread does not exceed 2 eV. At first glance this factor-of-10 finer resolution might imply that we should expect a few sharp spikes in the measured cross section, each several times larger than the broad peak predicted. However, since the overall enhancement is made up of numerous recombination resonances, each of which contributes to the total, accurate calculations of the individual resonances are needed to predict the expected enhancement at a specific energy in this experiment. Although no resonances of the predicted magnitude were observed, we do find small instabilities in the cross-section measurements, such as that seen at 805 eV, which lead us to suspect that resonances may indeed be contributing to the cross section. Over the remainder of the energy range studied, where resonant-excitation double autoionization is predicted to enhance the total cross section by 25% or less, the data can only lead to the general conclusion that the calculated direct cross section plus excitation-autoionization appears to slightly underestimate the measurements. Recent unpublished distorted-wave calculations³¹ for the direct ionization of Fe^{15+} are 15% lower than the Lotz prediction used by LaGattuta and Hahn. The use of these more accurate calculations for direct ionization would lower the direct plus excitation-autoionization sum by an additional 4%.

Indirect processes dominate the ionization of Fe^{15+} , with excitation-autoionization accounting for up to $\frac{3}{4}$ (or more) of the total cross section in the energy range studied here. Previous studies of the Na-isoelectronic sequence³⁶ revealed that the relative importance of indirect processes increased with increasing charge, and in fact on the basis of measurements through Si^{3+} it was predicted that excitation-autoionization contributions might be four times the direct cross section by Fe^{15+} . Depending on whether Lotz or the distorted-wave calculation is taken to estimate the direct-ionization contribution, the measurements indicate that excitation-autoionization contributes

3.5 to 4.5 times the direct cross section. The accuracy of the prediction in this case is encouraging but should not be taken for granted in more complex sequences.

IV. RATE COEFFICIENTS

It is expected that for many important applications the data presented here would be most useful in the form of rate coefficients. A computer program has been developed by the Controlled Fusion Atomic Data Center at Oak Ridge National Laboratory for the conversion of cross sections to rate coefficients and to provide convenient fits to the resulting rate-coefficient curves. The method of calculation³⁷ and fitting¹³ has been discussed. The Maxwellian electron-energy distributions had values of kT from 1 to 2×10^4 eV. The rate coefficients for each ion at selected energies are listed in Table IV and plotted in Fig. 6 along with the corresponding predictions of the commonly used Lotz rate-coefficient formula³⁴ and coefficients derived from rate measurements for Fe^{11+} by Brooks *et al.*³⁸

The natural logarithms of the rate coefficients listed in Table IV have been fitted to a Chebyshev polynomial expansion following the method reported by Cox and Hayes.³⁹ The fitting coefficients a_n ($n=0, 1, \dots, 8$) are listed in Table V and may be used to calculate the rate coefficients at any value of kT from E_{\min} to E_{\max} through a direct expansion of Chebyshev polynomials⁴⁰ of the first kind [$T_r(x)$] by the formula

$$\alpha(kT) = \exp \left[\frac{1}{2} a_0 + \sum_{r=1}^8 a_r T_r(x) \right], \quad (6)$$

where the rate coefficient α is in 10^{-10} cm^3/s , kT is in electron volts, and

$$x = \log \left[\frac{(kT)^2}{E_{\min} E_{\max}} \right] / \log \left[\frac{E_{\max}}{E_{\min}} \right], \quad (7)$$

TABLE IV. Maxwellian rate coefficients (in units of 10^{-10} cm^3/s) at selected values of kT (in eV) derived from the cross-section measurements.

kT (eV)	Fe^{11+}	Fe^{13+}	Fe^{15+}
7.0	0.000 00	0.000 00	
10.0	0.000 00	0.000 00	0.000 00
30.0	0.000 00	0.000 00	0.000 00
40.0	0.002 63	0.000 26	0.000 00
70.0	0.107	0.0209	0.000 69
100.0	0.493	0.128	0.0114
200.0	3.26	1.31	0.321
400.0	8.78	4.64	1.63
700.0	13.0	7.95	3.22
1000.0	14.7	9.72	4.25
2000.0	16.0	11.7	5.90
4000.0	15.2	11.7	6.78
7000.0	13.7	10.7	6.84
10000.0	12.5	9.78	6.60
20000.0	9.94	7.79	5.73

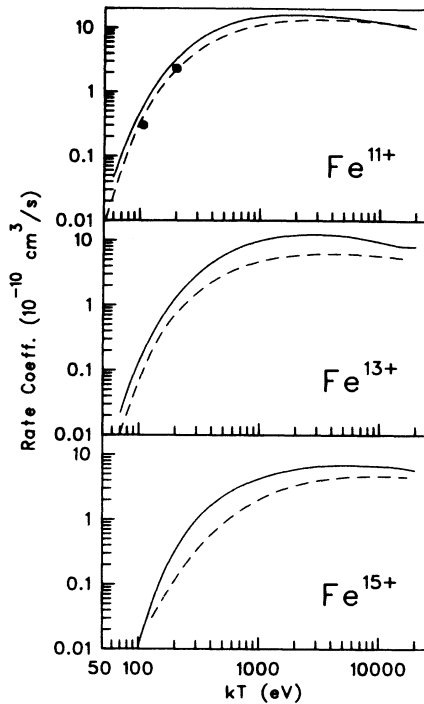


FIG. 6. Maxwellian rate coefficients for ionization of Fe¹¹⁺, Fe¹³⁺, and Fe¹⁵⁺. The solid curves were calculated based on the present data; the dashed curves are calculated from the Lotz formula for ionization rate coefficients (Ref. 34). The two solid circles are data of Brooks *et al.* (Ref. 38).

E_{\max} is 2×10^4 eV for each of these calculations, and E_{\min} is listed in Table V. Note that the rate coefficient is the exponential of the standard Chebyshev polynomial. The first eight Chebyshev polynomials are

$$\begin{aligned}
 T_1(x) &= x, \\
 T_2(x) &= 2x^2 - 1, \\
 T_3(x) &= 4x^3 - 3x, \\
 T_4(x) &= 8x^4 - 8x^2 + 1, \\
 T_5(x) &= 16x^5 - 20x^3 + 5x, \\
 T_6(x) &= 32x^6 - 48x^4 + 18x^2 - 1, \\
 T_7(x) &= 64x^7 - 112x^5 + 56x^3 - 7x, \\
 T_8(x) &= 128x^8 - 256x^6 + 160x^4 - 32x^2 + 1.
 \end{aligned} \tag{8}$$

TABLE V. Rate-coefficient fitting parameters. E_{\min} and E_{\max} (in eV) are the minimum and maximum values of kT over which the fit is valid; they are used to calculate the reduced energy x in the Chebyshev expansion (see text). Fitting parameters a_0 through a_8 are used in Eq. (6) to yield rate coefficients in units of 10^{-10} cm³/s.

Ion	E_{\min} (eV)	E_{\max} (eV)	a_0	a_1	a_2	a_3	a_4	a_5	a_6	a_7	a_8
Fe ¹¹⁺	7.0	20000.0	-60.810	17.313	-11.613	5.7283	-2.4257	0.90501	-0.29836	0.07059	-0.00476
Fe ¹³⁺	7.0	20000.0	-66.239	21.490	-14.252	7.1101	-3.0985	1.1778	-0.01560	0.06706	0.01560
Fe ¹⁵⁺	10.0	20000.0	-68.185	22.025	-14.182	6.8376	-2.7275	0.92152	-0.32611	0.13516	-0.05147

A computationally faster method of evaluating Chebyshev polynomials has been devised by Clenshaw,⁴¹ and the interested reader is referred to other sources for details¹³ and a sample program.³¹

The rate coefficients calculated from the present data are plotted in Fig. 6 along with predictions from the Lotz rate-coefficient formula.³⁴ For Fe¹¹⁺, the Lotz results are within 20% of the experimental values over most of the temperature range above 200 eV, and the curves converge at high temperatures. For Fe¹³⁺ and Fe¹⁵⁺, where indirect ionization makes a larger contribution to the total, the Lotz predictions are close to a factor of 2 lower over most of the temperature range plotted.

The only data available for comparison with the present measurements are rate coefficients for Fe¹¹⁺ derived from the time histories of emission lines in a small θ -pinch plasma by Brooks *et al.*³⁸ The two measurements (solid circles in Fig. 6), at effective temperatures of 105 and 200 eV, are in good agreement with predictions of the Lotz rate-coefficient formula, but are 30% lower compared to the values derived from cross-section measurements. This is better agreement than was found¹³ in a similar comparison for Fe⁹⁺. Both the θ -pinch and crossed-beam measurements are sensitive to highly excited metastable configurations found in Fe⁹⁺, and it is possible that a difference in a metastable content could account for some of the disagreement in that case.

V. SUMMARY AND CONCLUSIONS

Cross sections for ionization of Fe¹¹⁺, Fe¹³⁺, and Fe¹⁵⁺ have been presented, along with rate coefficients and fits to the rate coefficients. For Fe¹¹⁺, comparisons with theory suggest a significant metastable fraction in the incident ion beam, and calculated indirect ionization contributions to the total near the peak cross section are in good agreement with the experiment. Measurements and theoretical predictions are in good agreement for Fe¹³⁺ except that indirect ionization may be slightly larger than predicted by theory. Fe¹⁵⁺ measurements agree well with direct plus excitation-autoionization calculations. Predicted large enhancements of the total cross section due to resonant-excitation double autoionization are not observed at the expected levels, although indications of some resonance structures are found.

It is interesting to note that for Fe¹¹⁺ certain inner-shell transitions contribute to excitation-autoionization for metastable ions but not from the ground-state electron configuration. For some ions, indirect ionization may be

significantly different for ground-state and metastable configurations, so that the presence of metastables takes on added importance in determining accurate cross-section predictions. Excitation-autoionization is of increasing importance as this isonuclear sequence is followed from $11+$ to $15+$. This trend supports the rather broad generalization that indirect effects become more important in comparison with direct ionization as an isonuclear sequence is followed from inert-gas-like to alkali-metal-like electronic structure. Predictions of the importance of excitation-autoionization in the Na isoelectronic sequence for highly charged ions such as Fe^{15+} are borne out by the present data. These measurements, along with previous data and detailed calculations in the iron isonuclear sequence, provide a substantial data base of ac-

curate cross sections for plasma modeling, astrophysics, and fundamental atomic physics.

ACKNOWLEDGMENTS

The authors acknowledge valuable interactions with R. A. Phaneuf, D. C. Griffin, M. S. Pindzola, and C. Bottcher during this project. The permission to present cross-section calculations by M. S. Pindzola and rate-coefficient calculations and fits by H. T. Hunter prior to publication is also gratefully acknowledged. This work was supported by the Office of Fusion Energy, U.S. Department of Energy, under Contract No. DE-AC05-84OR21400 with Martin Marietta Energy Systems, Inc.

¹D. Palumbo, *Phys. Scr.* **23**, 69 (1971).

²C. F. Barnett, *Nucl. Instrum. Methods* **214**, 1 (1983).

³R. C. Isler, *Nucl. Fusion* **24**, 1599 (1984).

⁴R. C. Isler, R. V. Neidigh, and R. D. Cowan, *Phys. Lett.* **63A**, 295 (1977).

⁵V. P. Zhdanov, *J. Phys. B* **15**, L297 (1982).

⁶The name "resonant-recombination double autoionization" is recommended for this process in the report by C. Bottcher, D. C. Griffin, M. S. Pindzola, and R. A. Phaneuf, Oak Ridge National Laboratory Report No. ORNL/TM-8868, 1983 (unpublished), but "resonant excitation double Auger" from Ref. 19 is also used. "Resonant-excitation double autoionization," which is favored in Ref. 10, will be used here.

⁷R. A. Falk, G. H. Dunn, D. C. Gregory, and D. H. Crandall, *Phys. Rev. A* **27**, 762 (1983).

⁸D. C. Griffin, C. Bottcher, M. S. Pindzola, S. M. Younger, D. C. Gregory, and D. H. Crandall, *Phys. Rev. A* **29**, 1729 (1984).

⁹David H. Crandall, *Nucl. Instrum. Methods* **214**, 129 (1983).

¹⁰See, for example, G. H. Dunn, in *Electron Impact Ionization*, edited by T. D. Mark and G. H. Dunn (Springer-Verlag, Wien, 1985), pp. 277–316.

¹¹R. G. Montague, M. J. Diserens, and M. F. A. Harrison, *J. Phys. B* **17**, 2085 (1984).

¹²D. W. Mueller, T. J. Morgan, G. H. Dunn, D. C. Gregory, and D. H. Crandall, *Phys. Rev. A* **31**, 2905 (1985).

¹³D. C. Gregory, F. W. Meyer, A. Müller, and P. Defrance, *Phys. Rev. A* **34**, 3657 (1986).

¹⁴S. M. Younger, *J. Quant. Spectrosc. Radiat. Transfer* **29**, 61 (1983).

¹⁵D. C. Griffin, C. Bottcher, and M. S. Pindzola, *Phys. Rev. A* **25**, 1374 (1982).

¹⁶M. S. Pindzola, D. C. Griffin, and C. Bottcher, *Phys. Rev. A* **34**, 3668 (1986).

¹⁷J. B. Mann, *At. Data Nucl. Data Tables* **29**, 407 (1983).

¹⁸R. D. Cowan and J. B. Mann, *Astrophys. J.* **232**, 940 (1979).

¹⁹K. J. LaGattuta and Y. Hahn, *Phys. Rev. A* **24**, 2273 (1981).

²⁰K. T. Dolder and B. Peart, *Rep. Prog. Phys.* **39**, 693 (1976).

²¹M. F. A. Harrison, *Br. J. Appl. Phys.* **17**, 371 (1966).

²²F. Brouillard and P. Defrance, *Phys. Scr.* **3**, 801 (1983).

²³F. W. Meyer, *Nucl. Instrum. Methods Phys. Res.* **9**, 532

(1985).

²⁴P. O. Taylor, K. T. Dolder, W. E. Kauppila, and G. H. Dunn, *Rev. Sci. Instrum.* **45**, 538 (1974).

²⁵P. O. Taylor, thesis, University of Colorado, 1972.

²⁶This estimate is based in part on the resolution measured in unpublished work by D. S. Belic, R. A. Falk, G. H. Dunn, D. Gregory, C. Cisneros, and D. H. Crandall, *Bull. Am. Phys. Soc.* **26**, 1315 (1981).

²⁷D. H. Crandall, R. A. Phaneuf, and Gordon H. Dunn, *Phys. Rev. A* **11**, 1223 (1975).

²⁸J. N. Fox, R. L. Fitzwilson, and E. W. Thomas, *J. Phys. E* **3**, 36 (1970).

²⁹D. H. Crandall, J. A. Ray, and Carmen Cisneros, *Rev. Sci. Instrum.* **46**, 562 (1975).

³⁰Joachim Fricke, Alfred Müller, and Erhard Salzborn, *Nucl. Instrum. Methods* **175**, 379 (1980).

³¹M. S. Pindzola, D. C. Griffin, C. Bottcher, S. M. Younger, and H. T. Hunter, Oak Ridge National Laboratory Report No. ORNL/TM-10297, 1987 (unpublished).

³²D. C. Gregory, in *Electronic and Atomic Collisions*, edited by D. C. Lorents, W. E. Meyerhof, and J. R. Peterson (Elsevier, Amsterdam, 1986), pp. 205–214.

³³A. M. Howald, D. C. Gregory, F. W. Meyer, and R. A. Phaneuf, *Phys. Rev. A* **33**, 3779 (1986).

³⁴W. Lotz, *Z. Phys.* **220**, 466 (1969).

³⁵A. L. Mertz, J. B. Mann, W. D. Robb, and N. H. Magee, Jr., Los Alamos Scientific Laboratory Report No. LA-8267-MS, 1980 (unpublished), as reported in Ref. 19.

³⁶D. H. Crandall, R. A. Phaneuf, R. A. Falk, D. S. Belic, and G. H. Dunn, *Phys. Rev. A* **25**, 143 (1982).

³⁷D. H. Crandall, G. H. Dunn, A. Gallagher, D. G. Hummer, C. V. Kunasz, D. Leep, and P. O. Taylor, *Astrophys. J.* **191**, 789 (1974).

³⁸R. L. Brooks, R. U. Datla, A. D. Krumbein, and Hans R. Griem, *Phys. Rev. A* **21**, 1387 (1980).

³⁹M. G. Cox and J. G. Hayes, United Kingdom National Physical Laboratory Report No. NAC 26, 1973 (unpublished).

⁴⁰See, for example, *Handbook of Mathematical Functions*, edited by Milton Abramowitz and Irene A. Stegun (Dover, New York, 1970), p. 795.

⁴¹C. W. Clenshaw, *MTAC* **9**, 118 (1955).